Group 5:

Matthew Warner
CID: 01194459

Cameron Brown
CID: 01380114

Emiko Torii
CID: 01384560

Muhammad Aulia Rahman
CID: 01886324

Adam Wood
CID: 01351785

Submitted: 23/03/2021

Word Count: 6721

Future Clean Transport Technology Project 3: Modelling of lithium-ion batteries to understand limitations of performance

Executive Summary:
This report evaluates the performance of a Samsung INR18650-25R Li-ion cell by proposing and evaluating different models of increasing complexity.
Section 1 initialises the modelling using a Thévenin circuit with a simple voltage source and single fixed resistor. This model was found to be insufficient as, although it accounted for ohmic losses, it failed to consider the transient behaviour of the resistor nor the resistance from charge transfer and diffusion.
Following this, the second section of this report improves the accuracy of the model by introducing the first order ECM to predict the effect of transient behaviour and state of charge. The different battery characteristic at 0 °C, 20 °C, and 40 °C were used to find the temperature dependency of the battery. The comparison to the real test data was found to be slightly more accurate than the model in part 1 with the highest error of only about 5%.
Part three of the report introduces a thermally coupled model. It proves that, by considering only the reaction and the ohmic heat generation, the model can accurately predict the temperature variation of the cell during operation under passive air-cooling conditions.
Finally, the report concludes by adding SEI layer growth to the model. This has a large effect on standard operation, contributing to capacity fade and power fade via resistance increase. The latter of the two leads to the failure of the cell in under 8 years once the operating temperature exceeds 22°C, meaning an electric car manufacturer should not look to offer an 8-year warranty of a vehicle in a hotter location like New Delhi or Mecca. Additionally, they should neither offer such a warranty in colder locations like Nuuk, Greenland as sub-zero temperature will lead to premature cell failure from lithium plating.

Table of Contents

Nomenclature

Roman symbols	
Ah	**Energy Throughput**
i	**Current**
Q	**Cell Capacity**
R	**Resistance**
S_{loss}	**Capacity Loss**
t	**Time**
v	**Voltage**

Abbreviations	
ECN	**Equivalent Circuit Network**
SEI	**Solid Electrolyte Interphase**
SOC	**State of Charge**

Introduction

Lithium-ion batteries are the most applicable batteries for electric vehicle applications due to their high energy density and relatively long-life cycle. This battery, however, has dependency on many parameters such as the state of charge, temperature, and life cycle. One of the prominent parts of preparing and analysing the application of this battery is building an accurate model that can predict the behaviour of the battery based operational testing data.

In this report, a battery model of the Samsung INR18650-25R is built based on the training data and compared to the real test data obtained from an experiment. The models are built up from the simple ECN model, then improved by adding transient behaviour, current, temperature, and life cycle dependency to improve accuracy. This report is structured as follow:

- Part 1 of this report focuses on building a battery model with a simple equivalent circuit network (ECN). The discharge characteristic of the battery is obtained from the Samsung INR18650-25R specification sheet. The result obtained is then compared to the test data to indicate the accuracy of the model.
- Part 2 of this report explores the more complex first order ECN model which allows the model to display transient behaviour. The effect of current and temperature is introduced by obtaining the characteristic of the battery from the sets of training data at different temperatures. The accuracy of the prediction is then compared to the test data and the previous model discussed in part 1.
- Part 3 of this report introduces the thermal coupling in the model to increase the accuracy. Here, the previous temperature dependent model in part 2 is improved by taking the heat produced by the battery during the operation as one of the affecting parameters. The result is then plotted and compared to the test data as well as previously analysed models.
- Part 4 of this report analyses SEI layer growth's relationship with temperature. Cycle aging and calendar aging are considered for this model. By considering these processes in a single cell and determining critical values of resistance increase and capacity loss that would define end of life, the life of an electric vehicle battery can be predicted.

Figure 0.1 Samsung INR18650-25R Cell (eBike Batteries, 2019)

1. Equivalent circuit network modelling of a lithium ion battery - Thévenin Model

To begin the analysis, the Li-ion cell is simplified to a Thévenin circuit, a diagram of which can be seen below in figure 1.1.

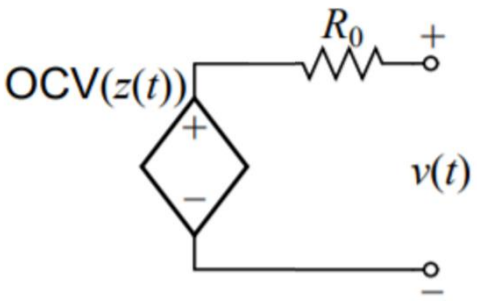

Figure 1.1 Equivalent Thévenin source model schematic

The equivalent resistance of this circuit, R_0, can be approximated from the discharge characteristics of the INR1860-25R cell in the provided Samsung spec sheet (Samsung SDI, 2013). The resistance was calculated as the mean of the ratios of voltage difference for two operating currents to the difference in said currents at 50% SOC. This process found R_0 to be 0.0183Ω.

To model SOC throughout the testing, equation 1.1 is used:

$$SOC(t+1) = SOC(t) - \frac{i(t)\Delta t}{Q} \tag{1.1}$$

where $i(t)$ is equal to the current at time t, Δt is the time step and Q is the total capacity of the cell. Using the data found within *SOC_OCV_MFCTT_2019,* the SOCs found using equation 1.1 are converted to OCVs, which are further converted to voltage using equation 1.2:

$$V(t) = OCV(t) - i(t)R_0 \tag{1.2}$$

The results of these predicted voltages, along with the actual values from *Battery_Testing_Data*, are plotted against time in figure 1.2. The data contains an initial resting period of 1.8 x 10^4 seconds which holds little importance and has thus been cropped from the plotted data.

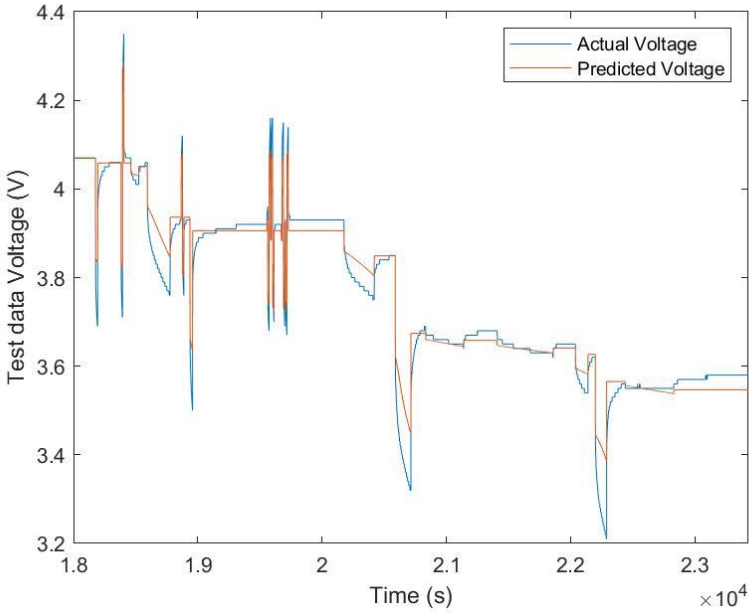

Figure 1.2 Predict and Actual voltage plotted against time

To provide further understand of the variation in actual and predicted voltage, figure 1.3 plots the error of the predicted voltage against time.

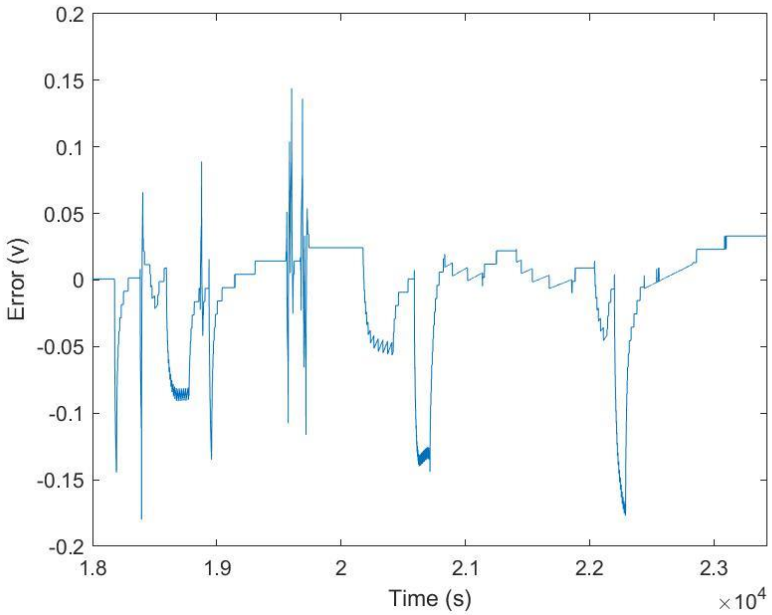

Figure 1.3 Error of predicted voltage against time

The largest errors found in both the positive and negative directions were found to be 0.145V at 1.96×10^4s and -0.181V at 1.844×10^4s respectively. The peaking in these errors appear to align with moments of rapid change from high current discharging to high current charging. To confirm this hypothesis, figure 1.4 overlays 1.3 onto a map of the test current profile.

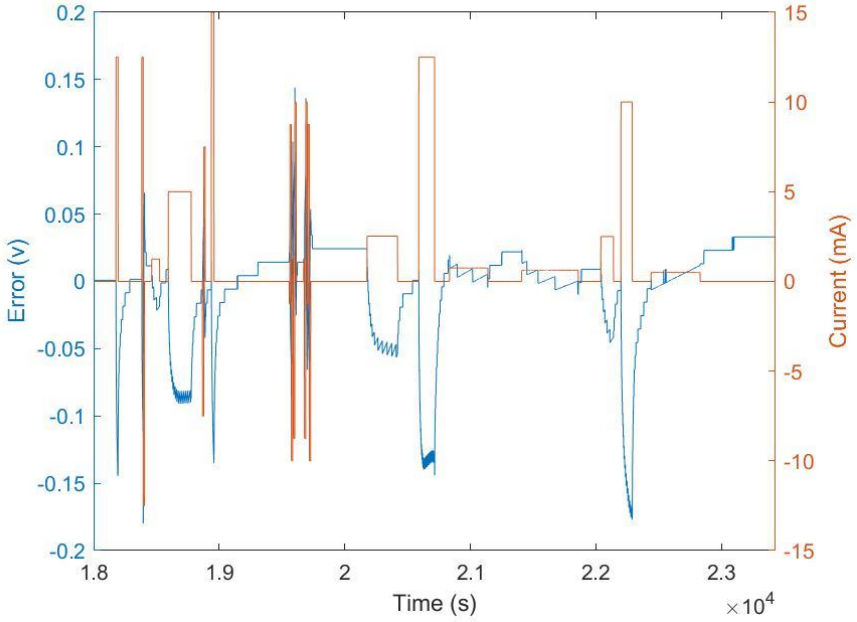

Figure 1.4 Voltage Error against Time compared to Current profile.

Here it can be seen that moments of rapid current change align with the largest errors in the voltage prediction, whereas current pulses with a longer duration lead to lesser, though not insignificant, levels of error. This is because the model currently being used does not consider the transient behaviour of the cell, and thus the true voltage sags behind the predicted voltage.

When considering the overall progression of errors over time, it can be difficult to make concrete assertions about whether there is a tendency for error to increase or decrease. Figure 1.5 plots a linear regression over the error plot from figure 1.3 and this regression line slopes upward, suggesting a general tendency for error to increase in the positive direction, albeit at a slow rate.

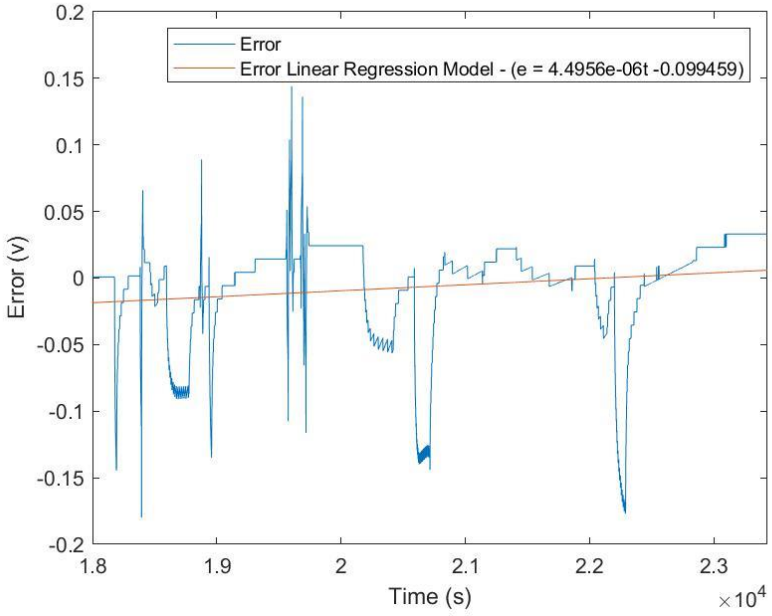

Figure 1.5 Linear Regression model fitted to Voltage Error against time

The errors come as a result of the oversimplification of the cell, namely the assumption made in defining the resistance. The model falls short as it only defines the resistance as being the ohmic losses of the system, whereas the real cell would encounter additional physical resistance such as resistance to charge transfer and diffusion resistance. A further oversight of this model is the fact that the resistance value is constant, thereby leading to the aforementioned negation of transient behaviour due to solid phase diffusion or double layer charging in addition of temperature sensitivity. The culmination of these factors can be seen by the general tendency of the error to increase over time along with momentary, large fluctuations.

2. Improvement of the model by introducing transient behaviour, current and temperature dependence

Part 2a: Transient behaviour and current dependence

Interpolating of parameters between values

When interpolating the values of parameters between measurement points, there are several approaches that can be used. Firstly, a lookup table can be created with the data at each measurement point so that linear interpolation can be used between the data points to obtain an approximate value for the parameter at the interpolation point. This is a simple approach and requires simple maths and little post processing of results but is only really accurate if the function describing the parameter is roughly linear or if the data points are sufficiently close together that a linear approximation between data points is reasonably accurate. This can require a large spread of data to be collected. Alternatively, the data can be fitted to a mathematical function. If the function is applied directly to find the parameter at the interpolation point, this can have the advantage of only needing to know the fitting equation to easily solve for the value of the parameter at any interpolation point. However, this method does require the knowledge of the behaviour of the parameter such that the data can be fitted to a sensible function. If the function is used to create a higher resolution lookup table then the error due to linear interpolation between data points decreases, but a knowledge of the behaviour of the parameter over the range of collected data is still required to fit the data to an appropriate function.

In this study, mathematical functions were used for fitting the data as the interpolation process. This is chosen not only because of the adequate knowledge of the behaviour of the parameter as a mathematical function, but also to increase the accuracy of the model compared to the validation data.

Fitting R_1 to a Gaussian function with current

The model training data was fitted to a first order ECN model with a resistor in series with a resistor and capacitor in parallel. A schematic of the equivalent circuit model is shown in Figure 2.1.

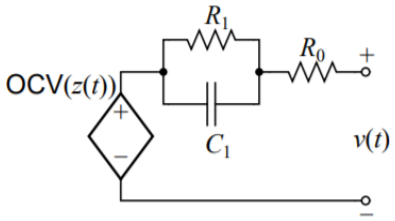

Figure 2.1 ECN model with sub-circuit

In order to fit the data to the model, the locations of key fitting points of the pulses in the model training data at 20 °C had to be recognised by the code. A plot of the training data with the important fitting points overlaid is shown in Figure 2.2. The three points of interest are the maximum/minimum voltage at the end of a charging/discharging pulse (red), the instantaneous voltage drop when current is switched to zero (yellow), and the first time that the voltage reaches its steady state value before the next pulse (green).

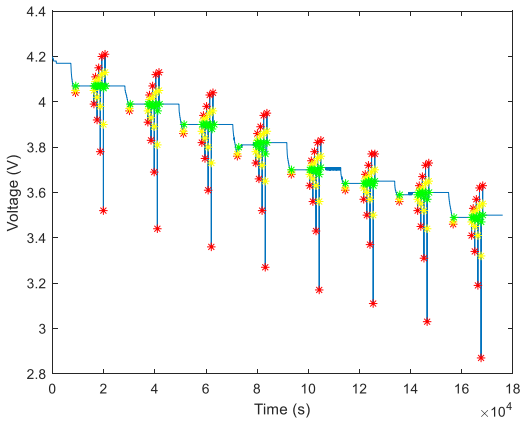

Figure 2.2 Model training data at 20 °C

R_0 was first calculated from the fitting data using Equation 2.1. The voltage difference between the red and yellow points marked on Figure 2.2 was divided by the current difference to find R_0 for each pulse.

$$R_0 = \frac{\Delta v_0}{\Delta i} \tag{2.1}$$

R_1 was then calculated using Equation 2.2 where v_∞ was taken as the difference in voltage between the red and green fitting points on the pulse shown in Figure 2.2 i.e., the total change in voltage once the current is removed at the end of the pulse.

$$R_1 = \frac{\Delta v_\infty}{\Delta i} - R_0 \tag{2.2}$$

Finally, the capacitance C_1 was calculated from Equation 2.3 where the time difference is taken between the red and green fitting points. This equation comes from the fact that the pulse response converges to steady state in about 4 time constants.

$$C_1 = \frac{\Delta t}{4R_1} \tag{2.3}$$

An average value of both R_0 and C_1 were then taken over all currents and SOCs and the model was refitted for R_1 using a constant value of R_0. We now had constant values for R_0 and C_1, but value for R_1 that change with both current and SOC.

$$Average\ R_0 = 0.0196\ \Omega, \qquad Average\ C_1 = 2455\ F$$

The obtained values were then fitted to first and second order Gaussian function as shown in Equation 2.4 and 2.5, respectively.

$$R_1 = R_1^{0A}.\exp^{-\frac{(I-b)^2}{c}} \tag{2.4}$$

$$R_1 = R_1^{0A}.\exp^{-\frac{(I-b_1)^2}{c_1}} + R_2^{0A}.\exp^{-\frac{(I-b_2)^2}{c_2}} \tag{2.5}$$

Where R^{0A} is the resistance at the open circuit, and b and c are fitting coefficient which do not have any physical meaning. The values of R_1 and Gaussian fittings were then plotted against current at 60% SOC as shown in Figure 2.3.

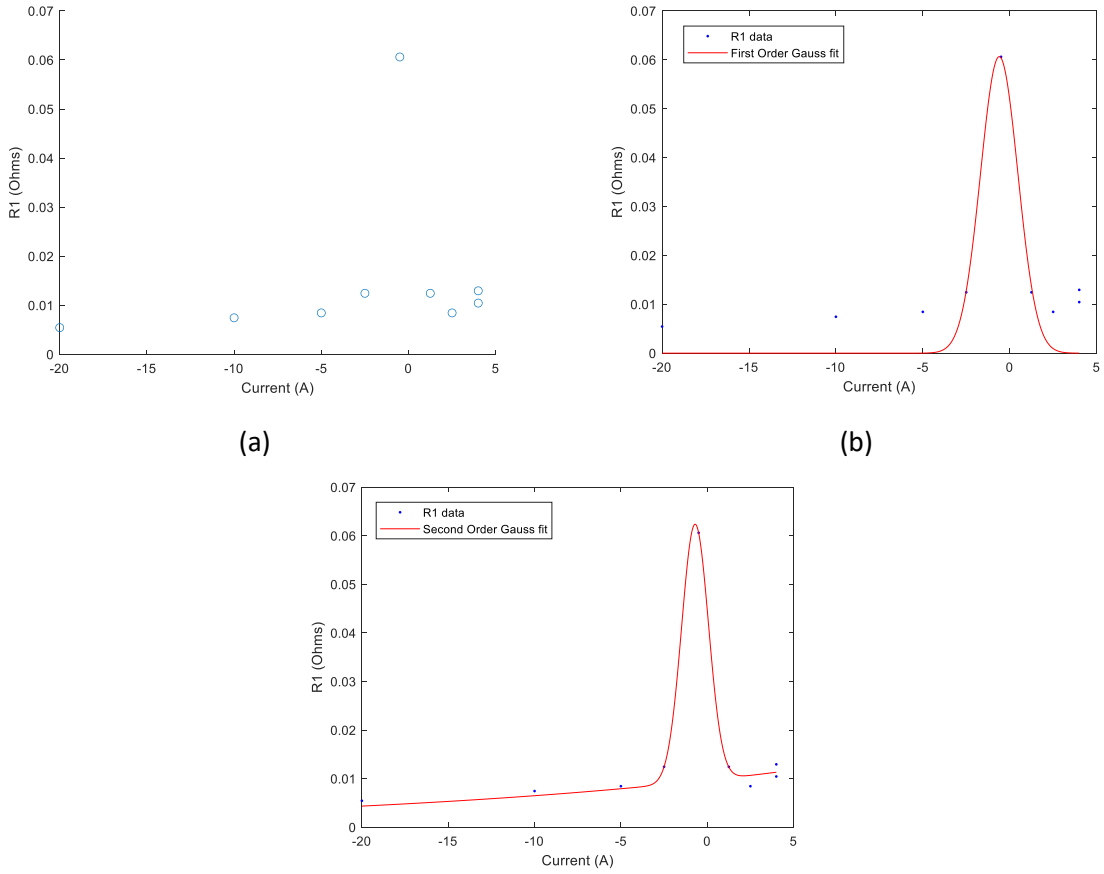

Figure 2.3 Plots of R1 for different current at 60% SOC as (a) real data, (b) first order Gaussian, and (c) second order Gaussian function

The data for R_1 resembles a normal distribution with maximum value somewhere close to zero current, and a roughly constant value at high charging or discharging currents. At first, the data was fitted to a first order Gauss function, but this failed to give a satisfactory fit, especially away from zero current where the predicted resistance would drop very quickly to zero. An improvement was made by fitting the data to a second order Gauss function instead. It should be noted that in order to obtain a good fit or the Gauss function, the value for R_1 associated with the slow discharge of the battery to 60% SOC was also used in the fitting of the function as there was a lack of data in the pulses for current values close to zero, especially for discharging.

By keeping the value of R_0 constant, we have essentially assumed that the ohmic resistance of the battery does not vary with the current being drawn by the external circuit or the state of charge of the battery. Figure 2.4(a) shows the value of R_0 as a function of current at 60% SOC. It seems that the assumption that R_0 does not vary with current is an accurate assumption as the value of R_0 remains around 0.02 Ω for all pulse currents.

By keeping C_1 constant we are assuming that the voltage relaxation at all currents and SOCs is broadly similar in that the time constant of the voltage relaxation only varies with R_1. A plot of C_1 against current is shown in Figure 2.4(b). From this plot is appears that the capacitance does vary with the current of the pulse as the calculated capacitance seems to be higher for lager currents in both the charging and discharging direction. This brings into question our assumption that C_1 is a constant. However, the approach used in this study to get the value of R_1, as shown in Equation 2.2, is independent of C_1. Hence, the fitting process shown in Figure 2.3 is still accurate.

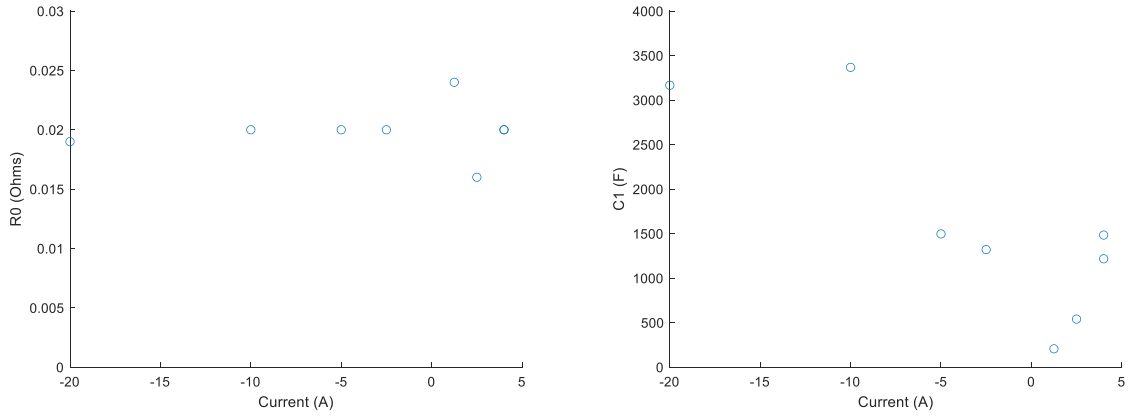

(a) (b)

Figure 2.4 Plots of (a) R_0 and (b) C_1 as the function of current at SOC 60%

Part 2b: Temperature dependence of R_0

Fitting the data for R_0 to an Arrhenius equation with temperature

The model training data for 0 °C and 40 °C was fitted using the same method as outlined above, but with the value of C_1 kept at the constant average value for 20 °C, throughout. The determined value of R_0 is plotted against temperature in Figure 2.5(a). From this figure, we can see that R_0 decreases at a decreasing rate, as the temperature of the battery increases. Therefore, an Arrhenius equation is a good approximation to the temperature dependence of R_0. The Arrhenius fitting function used for this model is shown in Equation 2.6.

$$R_0 = R_0^{20C} exp\left[-\frac{1}{R}\left(\frac{1}{T}-\frac{1}{T_0}\right)\right] \tag{2.6}$$

Where R_0^{20C} is the value of resistance obtained at 20 °C, T is temperature, R is gas constant, and E is fitting parameter. The fitted Arrhenius equation is shown overlaid on the R_0 data in Figure 2.5(b) and represents a decent fit for the measured data.

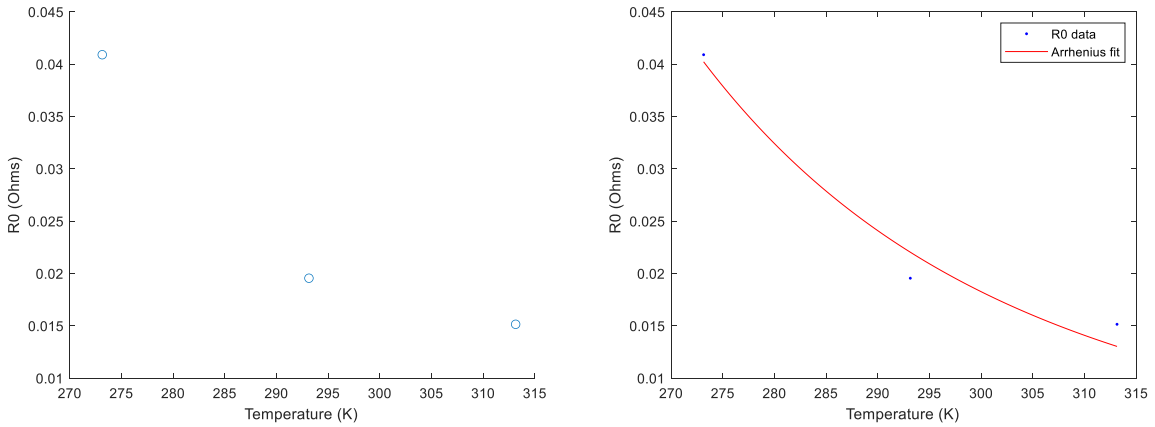

(a) (b)

Figure 2.5 Plots of R_0 as the function of temperature with (a) real data and (b) Arrhenius function

Clearly R_0 varies quite severely with temperature as over the temperature range of just 0-40 °C, R_0 decreases from 0.04 Ω to 0.015 Ω. This is a highly significant change in resistance over this temperature range. R_0 represents the ohmic resistance of the battery i.e., the resistance to electron and ionic flow within the cell. R_0 varies significantly with temperature because the electron mobility increases at higher temperatures. The increased electron mobility means that electrochemical reactions inside the cell happen faster so internal resistance is reduced. Higher temperatures also reduce the resistance of the electrolyte to ion flow at higher temperatures the ions move through the electrolyte more freely increasing the rate of electrochemical reactions and therefore reducing the internal ohmic resistance.

Part 2c: Temperature dependence of R_1

Fitting the data for R_1 to an Arrhenius equation with temperature

To determine how strongly R_1 depends on the state of charge of the battery, the value of R_1 at 0 °C and -2.5 A was plotted as a function of SOC. From Figure 2.6, R1 does show some dependency on the SOC. The value of R_1 appears to be higher at low states of charge compared to when the battery has a higher state of charge. R_1 seems to increase by over 100 % between 50% SOC and 20% SOC so if the true value of R_1 was to be modelled, the dependency on the SOC cannot be ignored. However, for the purposes of this fit, any dependence of R1 on SOC will be ignored.

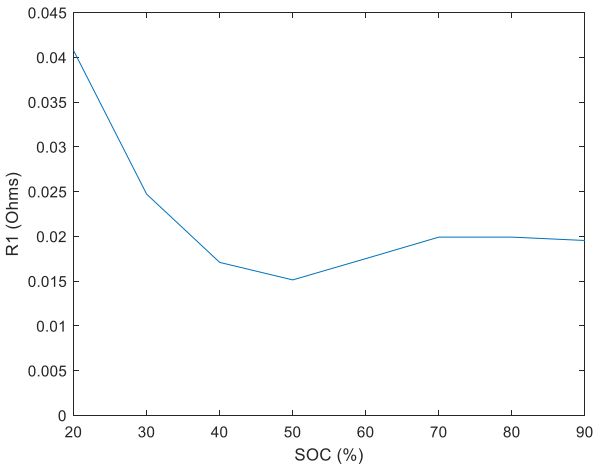

Figure 2.6 Plot of R_1 in the different SOC

The dependence of R_1 on temperature, however, cannot be ignored. Figure 2.7 show the value of R_1 at 60 % SOC and -2.5 A for each of the temperature. Similarly to the temperature dependency of R_0, R_1 also decreases as the temperature of the battery increases. R_1 is therefore also fitted to an Arrhenius equation which has been explained in Equation 2.5.

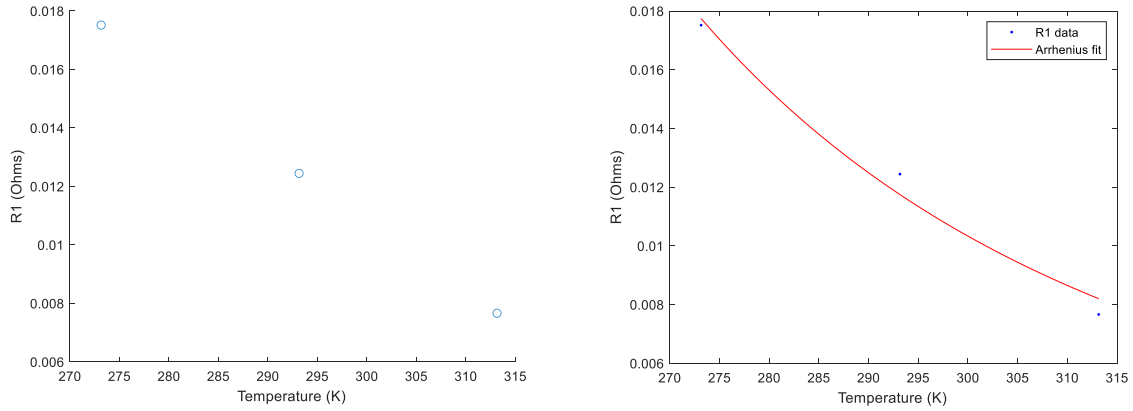

(a) (b)

Figure 2.7 Plots of R_1 as the function of temperature with (a) real data and (b) Arrhenius function

Figure 2.8 show the fit of the Arrhenius equation for R_1 to data for 30% and 90% SOC using the exponential constant determined at 60% SOC, but a pre-exponential factor of R_1 at the relevant SOC. The fit for R_1 looks pretty good at 90% SOC and seem so show similar error magnitudes of error to the original fit at 60% SOC. However, the accuracy of the fit is significantly reduced at 30% SOC, especially at low temperatures.

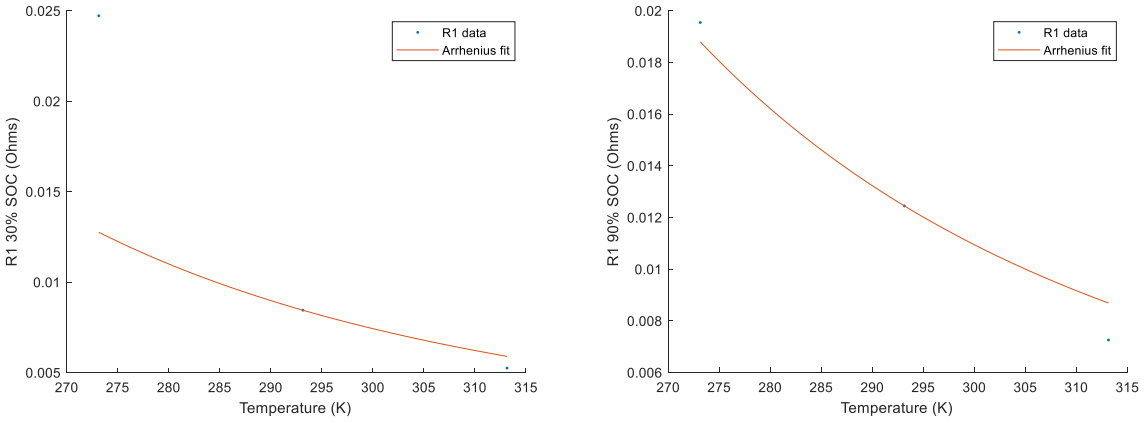

(a) (b)

Figure 2.8 Arrhenius fitting of R_1 in the different temperature at (a) 30% SOC and (b) 90% SOC

A refit of the average C_1 to the fitted data of R_0 and R_1 could produce a more accurate model, considering that the value of R_0 affects the value of R_1which further affects C_1.

Part 2d: Implementation

Implementing the model for comparison against battery testing data

Figure 2.9 shows the voltage against time predicted by our ECN model overlaid on the original battery testing data. Figure 2.10 shows a plot of the absolute error between our model and the testing data, against time. The largest error between the predicted and actual voltage is around 0.15 V which corresponds to a percentage error of only about 5% so the accuracy of our first order ECN model is quite good. The biggest error occurs in the region where the current is rapidly varying by large amounts. In this region, the current is rapidly cycling between -1 A and +1 A over a very short period of time and this pattern of rapidly varying current appears to cause the greatest error. The error in the model does not appear to be a function of the elapsed time as maximum error peaks coincide perfectly

with rapid changes in current, and when the current is not rapidly varying the absolute error is relatively low (only around 0.03 V).

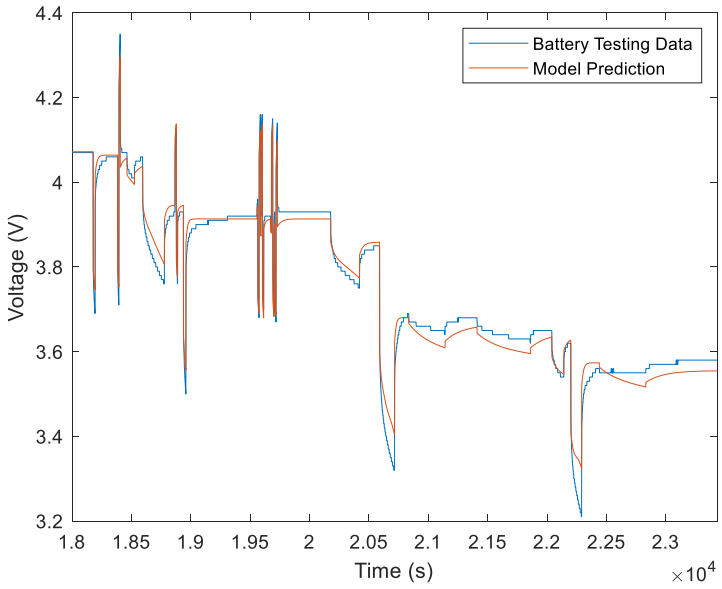

Figure 2.9 Voltage prediction of the model compared to the battery testing data

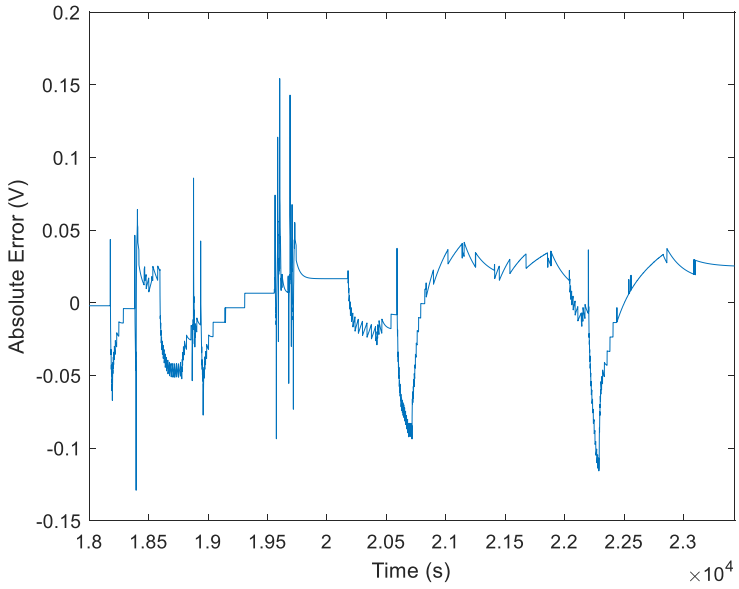

Figure 2.10 Absolute error of the voltage prediction of the model over time

Compared to the results in part 1, the first order ECN model shows a comparable error to the simple resistor model when current is changed rapidly. There is a slight improvement in error in these regions, but not by a large amount. The main improvement made by the first order ECN model appears to be when the current is varied more slowly and is not cycled between large positive and negative currents as seen by the reduction in error on the right side of the two error graphs.

The error, despite the higher order of the ECN of the model, still exists due to other assumptions made in the model. One way to increase the accuracy would be to the variation of C_1 over the temperature range.

3. Introducing a thermal model and thermal coupling

This section of the report discusses the thermal coupling of the model to predict the thermal behaviour of the cell. This was done by discretising the conservation of thermal energy equation for the cell and making the cell skin temperature the subject of the formula as is shown below in equation 3.1.

$$T_i = T_{i-1} + \frac{I^2 R_0 + I_1^2 R_1 - hA(T_{i-1} - T_{amb})}{mC_p} \tag{3.1}$$

, where:

Symbol	Parameter
T_i	Cell skin temperature at ith iteration
T_{i-1}	Cell skin temperature at $(\text{i-1})^{th}$ iteration
I	Series current
I_1	Current through resistor R_1 in parallel branch
R_0	Series resistor
R_1	Parallel resistor
h	Heat transfer coefficient
A	Surface area of the cell (found from the dimensions of the cell)
T_{amb}	Ambient temperature
m	Mass of the cell
C_p	Specific heat capacity of the cell

The heat generation of the cell is equal to the sum of the reaction heat and the ohmic heat. Furthermore, the cell was modelled as a lumped thermal mass and therefore the heat generation of the cell was assumed to be homogenous and distributed equally through the volume of the cell (not strictly true during normal operation).

Using the cell temperature at each iteration, the updated values for R_0 and R_1 were found at each time step. These updated values were used in a similar manner to as in part 2d to predict the output voltage of the cell for the given current profile at each time step. These results are shown below in Figure .

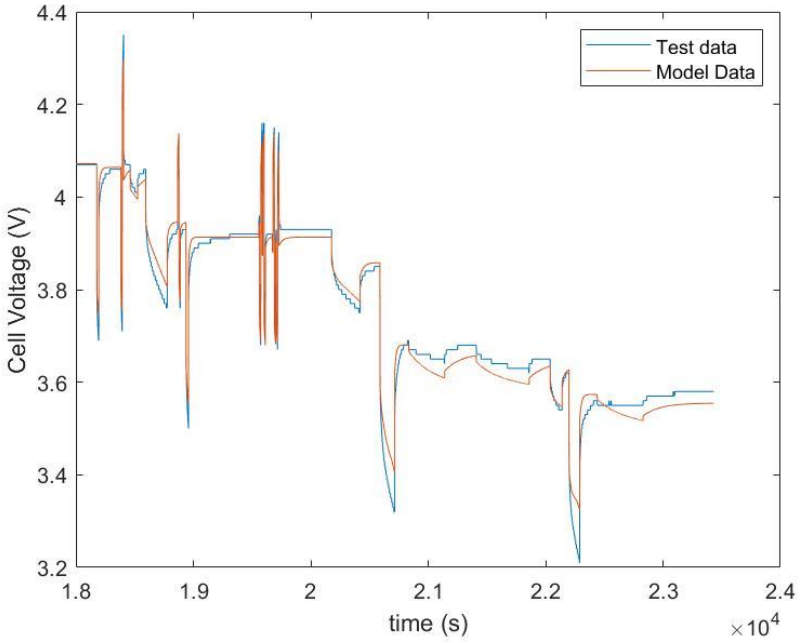

Figure 3.1 Graph of the cell voltage vs time for both the testing data and the data predicted by the model

Figure 3.2 shows a simple plot of the cell skin temperature vs time for both the test data and the temperature predicted by the model. We can see that the shapes of the curves are identical; however, the model data is translated vertically upwards to higher temperatures. This suggested that the value of h used initially was too small.

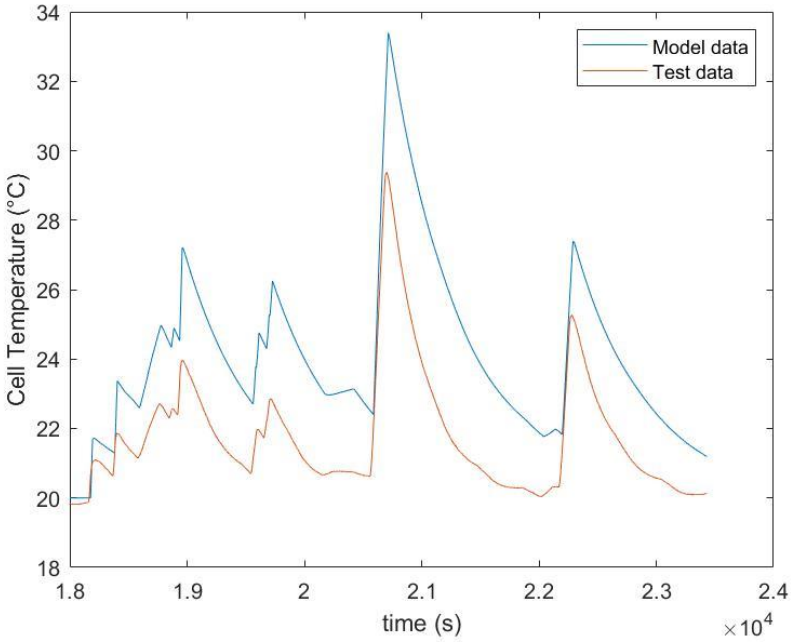

Figure 3.1 A graph of the cell skin temperature vs time for both the testing data and the data predicted by the model (h=10 W/(m^{2}K)

The value of h was adjusted in the code until the temperature curve predicted by the model matched that of the test data. This gave a value of 37 W K^{-1}m^{-2}. The curves can be seen to closely

follow each other except during the transient periods where the model seems to have a shorter time constant. The model is very accurate in predicting the peak temperatures reached by the cell.

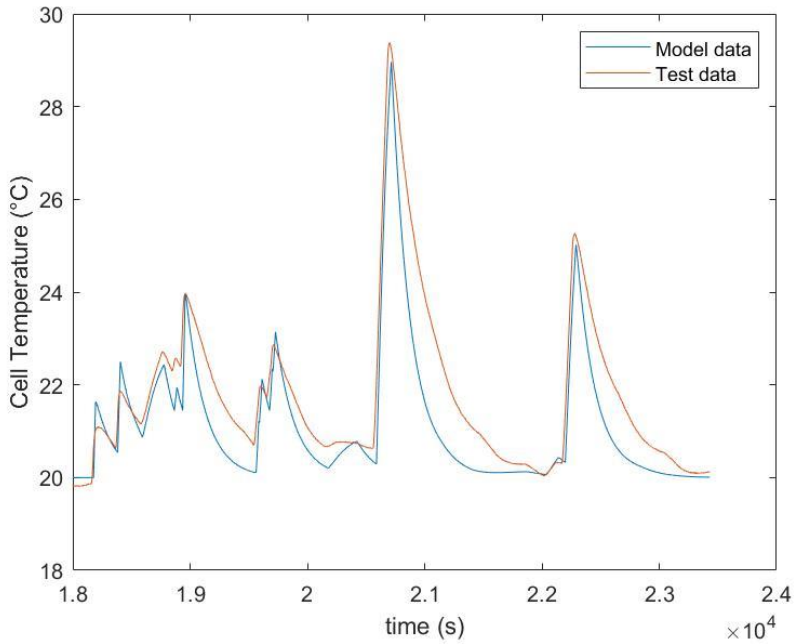

Figure 2.3 A graph of the cell skin temperature vs time for both the testing data and the data predicted by the model (h=37 W/(m2K))

The value of h required to match the test data temperature to the temperature predicted by the model was 37 W $K^{-1}m^{-2}$.

Table 3.1**Error! Reference source not found.** shows the heat transfer coefficients attainable for different convective conditions.

Table 3.1 - Convective heat transfer coefficients for different cooling methods (Vargas et al., 2018)

Conditions of heat transfer	[W·m^{-2}·K^{-1}]
Gases in free convection	5 – 37
Water in free convection	100 – 1200
Oil under free convection	50 – 350
Gas Flow in tubes and between tubes	10 – 350
Water flowing in tubes	500 – 1200
Oil flowing in tubes	300 – 1700
Molten metals flowing in tubes	2000 – 4500

The table**Error! Reference source not found.** suggests that the cell was cooled using passive air-cooling during testing. This was most likely carried out inside a climate chamber to ensure that the surrounding ambient air was kept at 20°C. If the cell was to be used inside a battery pack it is suggested that there be an active TMS to accurately control the temperature of the cell and prevent undesirable degradation during fast charging and discharging. This could be provided by direct liquid cooling (immersion cooling) or by indirect cooling via the base or surface of the cylindrical cells.
The error between the testing data temperature and the model predicted temperature was calculated and the time variation of this error is shown in the graph below.

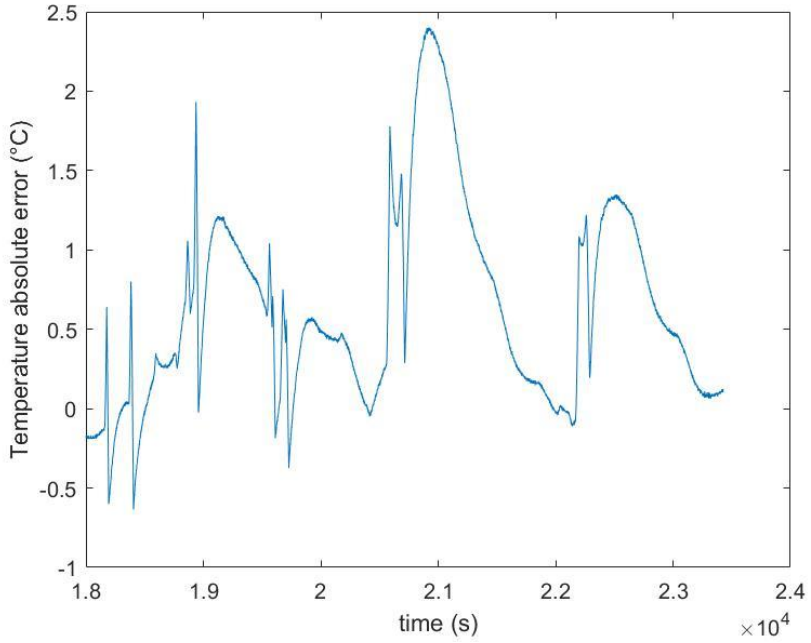

Figure 3.4 A graph showing the error between the temperature predicted by the model and the temperature recorded in the testing data

The error is shown to be very small when the charging and discharging currents are very small; however, the error becomes more important towards the end of the dataset where the magnitude of the currents is larger.

The model could be improved by using a climate chamber incorporating a more sophisticated control system such as PID control. The controller inside the climate chamber manages the ambient temperature of the chamber. If the controller is incapable of finely controlling the ambient temperature, then the testing data from which the model is trained is likely to have small errors. Bang-bang control simply switches on and off the temperature control unit when the ambient temperature goes above or below the bang-bang window. PID control offers a more accurate method of controlling the ambient temperature.

Returning to section 2c, the relationship between the resistance R1 and cell temperature was investigated. The discharge current was fixed to 20 A and three SOCs were investigated (30,60,90%) and plotted in figures 3.5-7

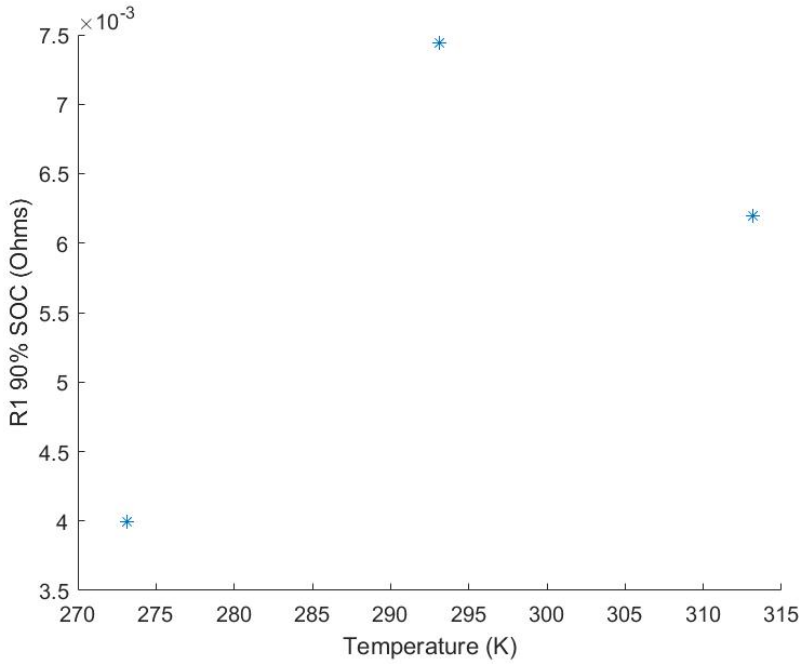

Figure 3.5 R1 vs Temperature at 20A discharge current and 90% SOC

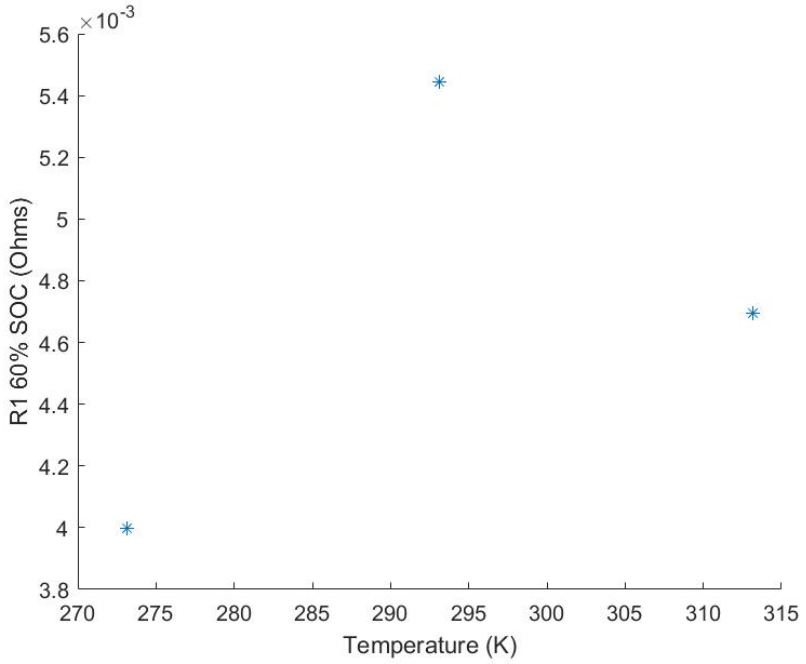

Figure 3.6 R1 vs temperature at 20 A discharge current and 60% SOC

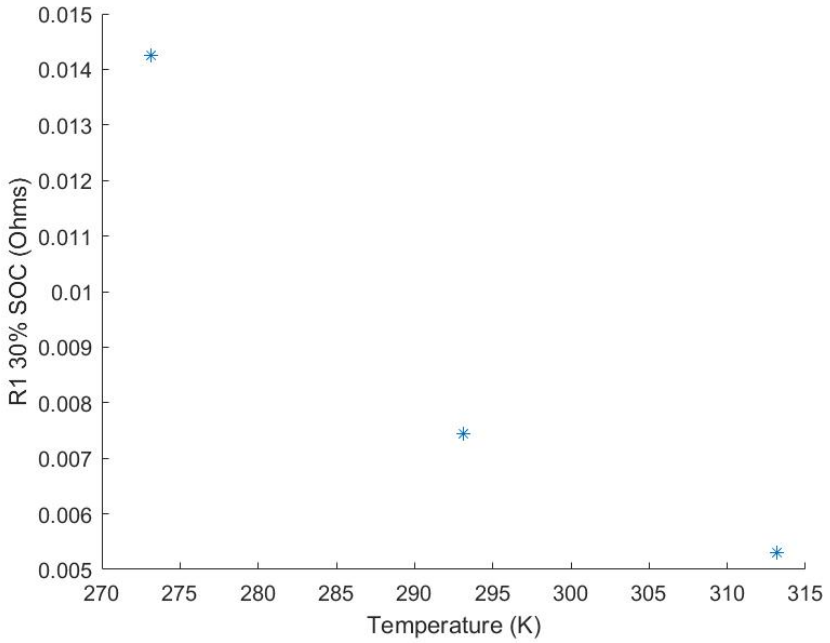

Figure 3.7 R1 vs temperature at 20 A discharge current and 30% SOC

By plotting the relationship between temperature and the value of R1 at -20A for each of the three SOCs, we can see that the data points at 0 °C don't match with what we would expect. It is expected that at the lowest temperature the R1 value should be the highest. This could be explained by low temperature performance effects in li-ion batteries. Lower temperatures are known to reduce the chemical reaction activity in addition to the ionic conductivity of the electrolyte. These effects are more pronounced at higher states of charge; therefore, the data point at 0 °C and 30% SOC behaves as expected.

4. Improvement of the model introducing a degradation mechanism

To improve the current model, degradation mechanisms can be added. The most dominant degradation mechanism under normal operating conditions is Solid Electrolyte Interphase (SEI) layer growth. The two principal effects this has on the battery is a reduction in capacity from lithium being consumed in the layer growth and a reduction in power as the cell's internal structure changes. These outcomes are known as capacity fade and power fade, respectively. Through understanding these two mechanisms we can attempt to model the degradation of cell over time. Capacity fade (S_{loss}) has experimentally been found to relate to power throughput and temperature by the function described in equation 4.1, while the power fade (R_{inc}) was found to have a similar relationship to these variables as seen in equation 4.2.

$$S_{loss\ cycle} = a_c e^{-\frac{E_{ac\ resistance}}{RT}} Ah^{z_{cycle}} \tag{4.1}$$

$$R_{inc\ cycling} = a_R e^{-\frac{E_{ac\ Capacitance}}{RT}} Ah \tag{4.2}$$

Where a_c and a_r are fitting constants, E_{ac} is activation energy, R is the universal gas constant, T is temperature, Ah is energy throughput, and z is a power exponent. Following similar relationships to these, capacity fade and power fade in storage can also be calculated from equations 4.3 and 4.4, respectively.

$$S_{loss\ calendar} = b_c e^{-\frac{E_{ac\ Capacitance}}{RT}} t^{z_{calendar}} \tag{4.3}$$

$$R_{inc\ calendar} = b_R e^{-\frac{E_{ac\ resistance}}{RT}} t \tag{4.4}$$

Where b_c and b_r are fitting constants, $time$ is time spent in storage – the key factor differing these relationships from those used in cell cycling. Using the raw data from the Samsung 25R cell and the values of $E_{ac\ resistance}$, $E_{ac\ capacitance}$ and z_{cycle} found within Cordoba-Areanas et al.(2014) (values seen in table 4.1), the optimal values for a_c, a_R, b_c, and b_R can be found through the use of MATLAB's *fittype* function. The raw cell data could be used to find energy throughput by multiplying the number of cycles by 5Ah which represents the 2.5Ah charge and 2.5Ah discharge at 100% DoD for one cycle.

Table 4.1: Model Constants for Equations 4.1-4	
$E_{ac\ resistance}$	51800 J/mol
$E_{ac\ Capacitance}$	22406 J/mol
z_{cycle}	0.48

There are some drawbacks to using the data in this way. The means of establishing energy throughput fails to consider the effects of capacity fade, resulting in the energy throughput being higher than is realistic. Additionally, 100% DoD is not a realistic use case as over-charging and discharging should be avoided to prevent exaggerated degradation. When considering the error surrounding these fittings, one of the key considerations is the time steps used. If the model were only to be updated every hour, this may not be able to capture small changes in the measured quantity. Furthermore, larger time steps for the same length of time will result in a smaller number of data points being available to fit the model to, ultimately reducing the accuracy of the fitting. The aforementioned equations were fitted to datasets at 45°C and 60°C and are displayed graphically with their respective datasets below in figures 4.1-4.4.

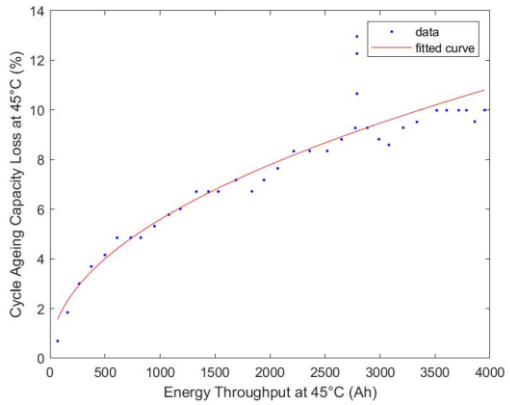

Figure 4.1 Fitted Equation 4.1

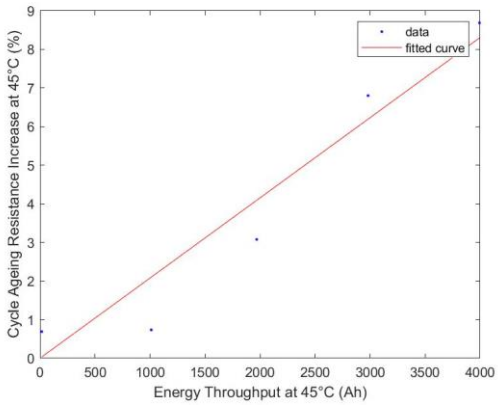

Figure 4.2 Fitted Equation 4.2

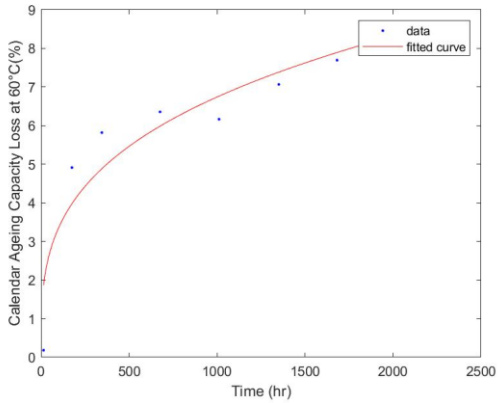

Figure 4.3 Fitted Equation 4.3

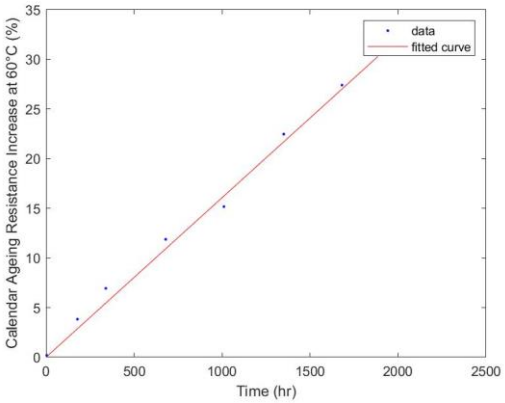

Figure 4.4 Fitted Equation 4.4

Based on visual observations alone, the models appear to fit the dataset to an acceptable degree. One possible complaint to be had with the model is the fact that it does not cover a particularly great length of time and thus it may present some inaccuracies as the model is extrapolated out. Nonetheless, these models are now available to be used to predict battery performance. Figure 4.5 plots capacity loss against energy throughput assuming that the cell is being cycled continuously for 5,000 hours at 1C/1C charge/discharge from 10°C to 60°C (283.15K to 333.15K) at 10°C increments. It should be noted that these temperatures represent the external ambient temperatures and therefore neglect the internal temperature of the cell and any effects this can have on the air temperature.

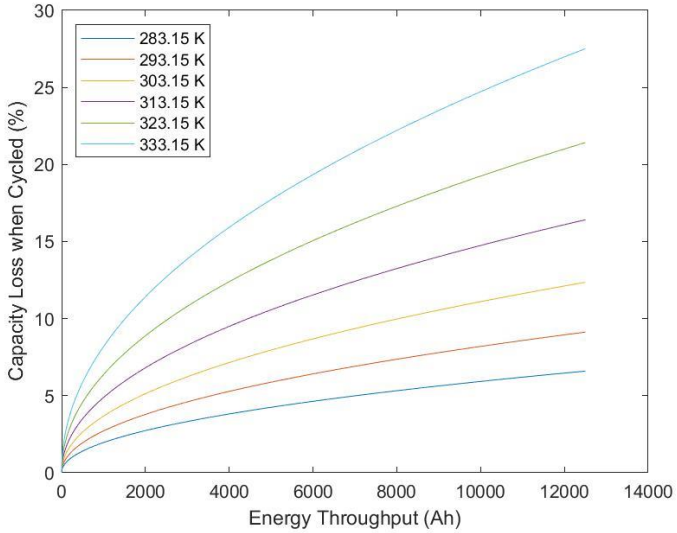

Figure 4.5 Capacity Loss Against Energy Throughput for 5000 hours of continuous cycling at varying Temperatures

Similarly, figure 4.6 similarly shows resistance increase against energy throughput over the same variable ranges.

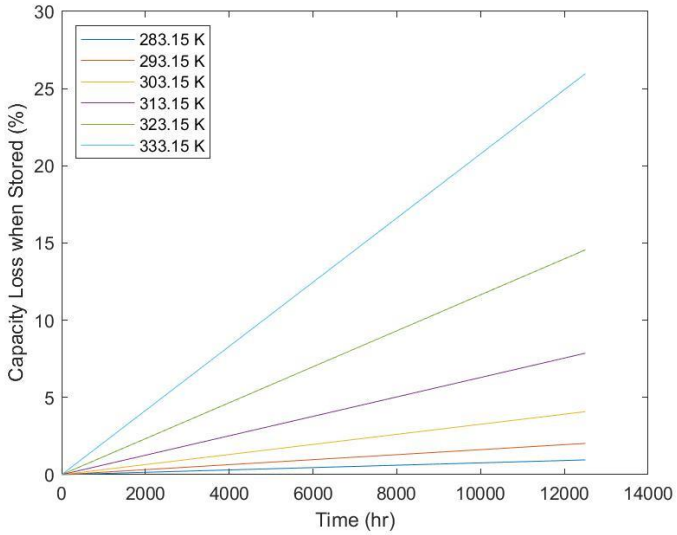

Figure 4.6 Resistance Increase Against Time for 5000 hours of continuous Cycling at Varying Temperatures

The fitted models also allow for predictions to be made regarding the degradation in storage. Figures 4.7 and 4.8 display capacity loss and resistance increase against storage time assuming that the cell is being stored for 10 years at 10°C to 60°C at 10°C increments, respectively.

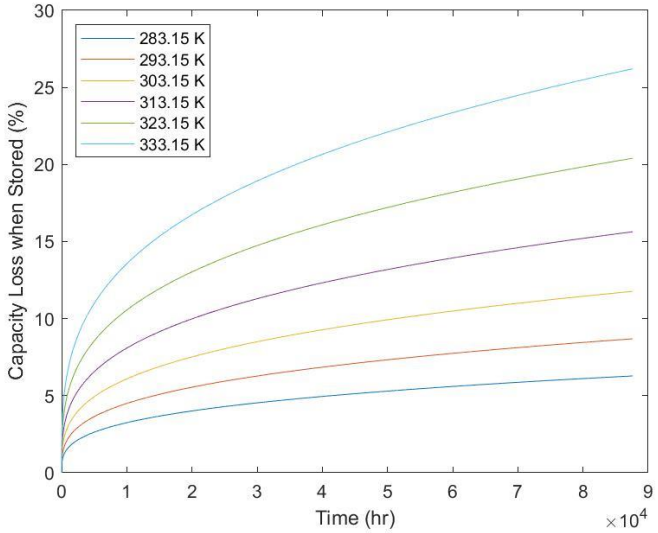

Figure 4.7 Capacity Loss against Time in Storage of 10 years at varying Temperatures

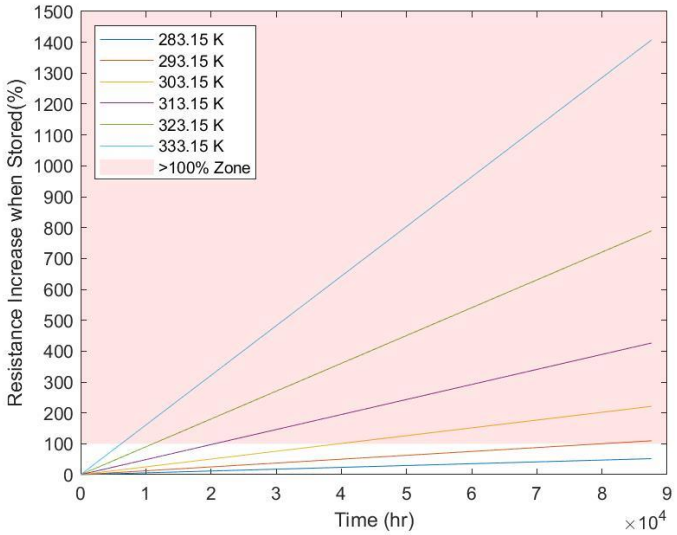

Figure 4.8 Resistance Increase against Time in Storage over 10 years at varying Temperatures, with marked Failure Zone

These models can be put to use to in estimating the life of an electric vehicle battery pack if end of life is defined as the capacity fading by 30% or the resistance increasing by 100%. Furthermore, in order to use these models to make such predictions it must be assumed that one cell is representative of every cell in the pack simultaneously and that the vehicle will by cycled continuously at 1C/1C. The first of these assumptions is fair as battery packs in these applications will have a Battery Management System (BMS) that will make the individual cells operate in this way. Buchmann (2020) suggest the second assumption is valid also, so long as the difference discharge profiles between the test data and real vehicle usage can be accepted.

Returning to figures 4.5 to 4.8 which display capacity loss and resistance increase, it can be identified that the failure mechanism that will cause end of life will be resistance increase as capacity losses never reach the critical value for failure in the 10 years of storage or 5000 hours of cycling. Additionally, the resistance loss due to cycling also does not lead to end of life within 5000 hours either. The dominant process determining end of life appears from figure 4.8 to be resistance

increases in storage. The time until the critical value of resistance increase was reached at each temperature can be seen in table 4.2.

Table 4.2 - Hours until battery failure at different temperatures

Average Temperature(K)	Hours Storage until Failure (hrs)
283.15	>87600
293.15	79842
303.15	39605
313.15	20546
323.15	11101
333.15	6223

As an inspection of the governing equation (4.4) would suggest, in increase in temperature leads to faster degradation of the cell, thereby reducing expected battery life with increasing temperature. This is not the only temperature that should be considered, however. Wu et al. (2020) find that battery degradation at sub-zero temperatures actually increases as lithium in the cell begins to precipitate, causing a loss in active lithium. This factor is not considered in the model. Furthermore, unless the vehicle is kept as a showpiece and is never driven it is unreasonable to assume the resistance increase would follow the storage model alone. The real-life expectancies of the batteries would be lower than those in table 4.2 as some amount of resistance increase from cycling would cause the critical value to be met sooner.

If it is assumed that the vehicle spends 95% of its time parked and the remaining 5% in a state of cycling charge/discharge then more comprehensive statements on the life of the battery can be made. Table 4.3 holds the average temperatures of major cities around the world as well as the length of time it would take for an electric vehicle battery in that environment to reach the end of its life, assuming the aforementioned 95-5% split assumption. These times are found from the combined resistance of increase from both storage and cycling. The progression of these degradations can be seen plotted in figure 4.9.

Table 4.3 - Hours until battery failure in different global cities (Wikipedia, 2021)

City, Country	Average Temperature(K)	Hours Storage until Failure (hrs)
Edinburgh, UK	282.45	>87600
Washington D.C., USA	287.75	>87600
Brasília, Brazil	293.75	79127
New Delhi, India	298.15	57861
Mecca, Saudi Arabia	323.15	39362

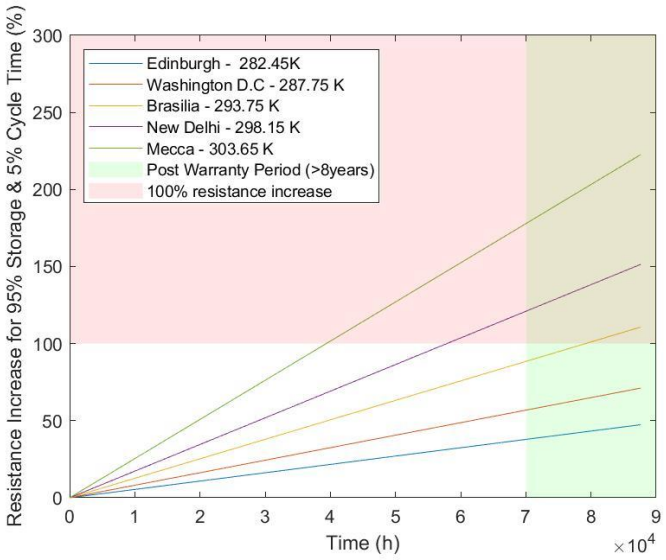

Figure 4.9 Graph of total battery degradation against time in different global cities

It should be noted that these values are calculated by assuming a single, continuous temperature throughout the year. The true temperature that the batteries would experience would in reality be roughly sinusoidal around this value. Given that the equations 4.1-4.4 suggest all forms of degradation will increase exponentially with temperature increase, the true rate of degradation would likely be faster than this model predicts but would be impossible to accurately predicted without detailed temperature records/ predictions and model of complexity beyond the scope of this report.

Given that an electric vehicle battery will last for different lengths of time around the world, it could be useful as a car manufacturer to know in what parts of the world it would be appropriate to sell electric vehicles with an eight-year warranty – if the city is of a temperature that meets the red zone of figure 4.9 before the green zone then there will be an abundance of customers will be claiming the failure of the batteries against their warranty. As is displayed in figure 4.10, the critical temperature at which a cell will not last more than eight years (to the nearest degree) is 22°C or 295.15K.

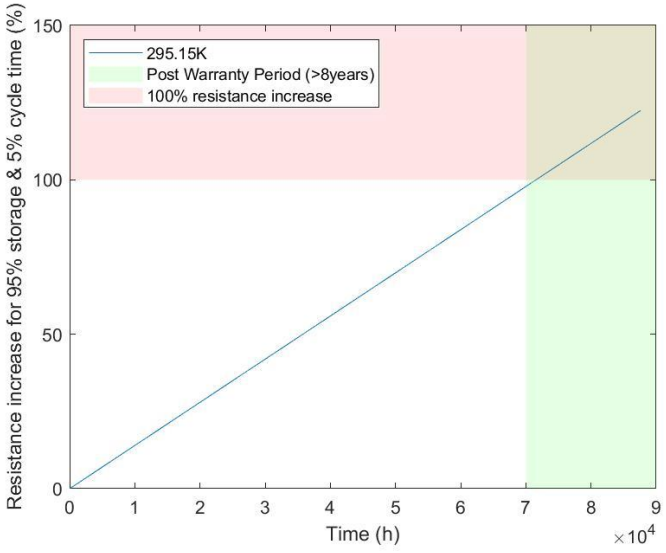

Figure 4.10 Graph of battery degradation for battery at optimal temperature for 8-year life

This means the 8-year warranty offer would be acceptable in cooler cities such as Edinburgh or Washington, but unsustainable in hotter cities like New Delhi and Mecca. Additionally, manufactures should avoid selling electric vehicles with this warranty in cities the experience periods of prolonged, extreme cold such as Nuuk in Greenland, which experiences an average annual temperature of -1.4°C (Wikipedia, 2021), as Lithium plating will also lead to a decreased battery life.

Conclusions

This report set out with the objective of producing a model around a Samsung INR18650-25R Li-ion battery. The first section of this report set the groundwork for this, implementing a Thévenin source approximation consisting of a voltage source and a single resistor in series. The predictions made by this model were compared to real battery performance data. The residuals between these two datasets varied wildly over time, with a slight trend in the direction of positive error. The largest errors were found to exist at moments of sudden current pulses, whereas more steady periods of current aligned with more stable errors. This model was ultimately considered inadequate as it did not consider a number of factors that were contributing to its error such as resistor transient behaviour or temperature dependence.

In section 2, the battery model was improved by introducing the effect of transient behaviour, state of charge, and temperature on the battery performance. First order ECN was used in this model. The battery characteristics were extracted by analysing battery training data obtained from the experiment. Those values were then fitted using second order Gaussian and Arrhenius function for fitting process for each current and temperature, respectively. The result shows a good accuracy, with the maximum error of only about 5%. Compared to the results in part 1, this model shows a slight improvement but not by a large amount. The main reduction of error was when the change of voltage occurs slowly. The error in the point where the voltage has a sudden change, however, still have relatively large error.

Section 3 investigated the effects of coupling a thermal model with the electrical model developed from the previous sections. The temperature of the cell was used to update the values of R0 and R1 at each time step. From these values the ohmic and reaction heats were calculated and, using heat transfer conservation equations a new cell temperature was found at each time step. This meant that the values of R0 and R1 were calculated from the rolling temperature profile of the cell. The value of convective heat transfer coefficient, h, for the cell was found to be 37 W/m^2K which proved that the cell had been tested in a climate control chamber under passive air cooling. It was suggested that if the cell was to be operated at high discharge rates, then a more powerful thermal management system be designed to remove sufficient heat from the cell. Finally, it was suggested that in order to reduce the temperature error between the temperature predicted by the model and the testing data, that a more sophisticated temperature control algorithm, such as PID, be used to accurately control the ambient temperature in the climate chamber.

Finally, section 4 rounds off the modelling by factoring in the consideration of SEI layer growth's relationship with temperature. Two degradation models were considered for this relationship – cycle aging and calendar aging. By considering these processes in a single cell and determining critical values of resistance increase and capacity loss that would define end of life, the life of an electric vehicle battery could be predicted. Although both failure mechanisms were highly temperature dependant, it was found that the effects of resistance loss overpower those of capacity loss, resulting in batteries in consistent temperatures above 22°C failing in under 8 years. This information could provide valuable insight to car manufactures/dealers, as offering 8-year warranties on electric vehicles hotter cities such as Mecca and New Delhi would not be as sustainable of a business decision as in cooler cities such as Edinburgh and Washington D.C.

References

Buchmann, I., 2020, *BU-1004: Charging an Electric Vehicle*, Viewed 12 March 2021, <https://batteryuniversity.com/learn/article/bu_1004_charging_an_electric_vehicle>.

Cordoba-Arenas, A., Onori, S., Guezennes, Y. & Rizzoni, G., 2014. 'Capacity and power fade cycle-life model for plug-in hybrid electric', *Journal of Power Sources* 278, pp. 473-483.

eBike Batteries, 2019, *Samsung INR18650-25R 20A 2500mAh,* Viewed 16 March 2021, <https://ebikebatteries.co.uk/product/samsung-inr18650-25r-20a-2500mah/>.

Samsung SDI, 2013, *Introduction of INR18650-25R,* Samsung SDI Co. Ltd.

Vargas, R., Gonda, V. & Ruiz, L., 2018, *Thermal analysis and control for heating of an extrusion die*. 1.

Wikipedia, 2021. *List of cities by average temperature*, Viewed 15 March 2021, <https://en.wikipedia.org/wiki/List_of_cities_by_average_temperature>.

Wu, X. et al., 2020*, '*Study on the Capacity Fading Effect of Low-Rate Charging on Lithium-Ion Batteries in Low-Temperature Environment'*, World Electric Vehicle Journal 11(3):55.*